

1 The characteristics of atmospheric brown carbon in Xi'an,  
2 inland China: sources, size distributions and optical properties

3  
4  
5  
6  
7 Can Wu<sup>1,2</sup>, Gehui Wang<sup>1,2,3,4\*</sup>, Jin Li<sup>2</sup>, Jianjun Li<sup>2</sup>, Cong Cao<sup>2</sup>, Shuangshuang Ge<sup>1</sup>, Yuning  
8 Xie<sup>1</sup>, Jianmin Chen<sup>3,5</sup>, Xingru Li<sup>1,6</sup>, Guoyan Xue<sup>1</sup>, Xinpei Wang<sup>1</sup>, Zhuyu Zhao<sup>7</sup>, Fang Cao<sup>7</sup>  
9

10  
11  
12  
13  
14  
15 <sup>1</sup>Key Lab of Geographic Information Science of the Ministry of Education, School of  
16 Geographic Sciences, East China Normal University, Shanghai 210062, China

17 <sup>2</sup>Key Lab of Aerosol Physics and Chemistry, State Key Laboratory of Loess and Quaternary  
18 Geology, Institute of Earth Environment, Chinese Academy of Sciences, Xi'an 710061,  
19 China

20 <sup>3</sup>Institute of Eco-Chongming, 3663 North Zhongshan Road, Shanghai 200062, China

21 <sup>4</sup>CAS Center for Excellence in Regional Atmospheric Environment, Institute of Urban  
22 Environment, Chinese Academy of Sciences, Xiamen 361021, China

23 <sup>5</sup>Department of Environmental Science and Technology, Fudan University, Shanghai 200433,  
24 China

25 <sup>6</sup>Department of Chemistry, Analytical and Testing Center, Capital Normal University, Beijing  
26 100048, China

27 <sup>7</sup>Yale-NUIST Center on Atmospheric Environment, Nanjing University of Information  
28 Science & Technology, Nanjing 210044, China  
29  
30  
31  
32  
33  
34

35 \*Corresponding author. Prof. Gehui Wang

36 E-mail address: [ghwang@geo.ecnu.edu.cn](mailto:ghwang@geo.ecnu.edu.cn), (Gehui Wang)  
37  
38  
39

40 **Abstract:** To investigate the characteristic of atmospheric brown carbon (BrC) in the  
41 semi-arid region of East Asia, PM<sub>2.5</sub> and size-resolved particles in the urban atmosphere of  
42 Xi'an, inland China during the winter and summer of 2017 were collected and analyzed for  
43 optical properties and chemical compositions. Methanol extracts (MeOH-extracts) were more  
44 light-absorbing than water extracts (H<sub>2</sub>O- extracts) in the optical wavelength of 300-600 nm,  
45 and well correlated with nitrophenols, polycyclic aromatic hydrocarbons (PAHs) and  
46 oxygenated PAHs ( $r > 0.78$ ). The light absorptions ( $abs_{\lambda=365nm}$ ) of H<sub>2</sub>O- extracts and  
47 MeOH-extracts in winter were  $28 \pm 16$  M/m and  $49 \pm 32$  M/m, respectively, which are about 10  
48 times higher than those in summer, mainly due to the enhanced emissions from biomass  
49 burning for house heating. Water extracted BrC predominately occurred in the fine mode ( $<$   
50  $2.1 \mu m$ ) during winter and summer, accounting for 81% and 65% of the total absorption of  
51 BrC, respectively. The light absorption and stable carbon isotope composition measurements  
52 showed an increasing ratio of  $abs_{\lambda=365nm}$ -MeOH to  $abs_{\lambda=550nm}$ -EC along with an enrichment of  
53 <sup>13</sup>C in PM<sub>2.5</sub> during the haze development, indicating an accumulation of secondarily formed  
54 BrC (e.g., nitrophenols) in aerosol aging process. PMF analysis showed that biomass burning,  
55 fossil fuel combustion, secondary formation, and fugitive dust are the major sources of BrC in  
56 the city, accounting for 55%, 19%, 16%, and 10% of the total BrC of PM<sub>2.5</sub>, respectively.

57

58 **Key words:** Brown Carbon; Haze; Stable carbon isotope composition; Biomass burning;  
59 Secondary formation.

60

61

## 62 **1. Introduction**

63 Brown carbon (BrC) is a vital fraction of carbonaceous aerosols, and exhibits strong  
64 absorption ability from near ultraviolet (UV) to visible light region. Thus, it has been given  
65 extensive investigation in the recent decades (Laskin et al., 2015; Yan et al., 2018; Gustafsson  
66 et al., 2009). BrC has significant impact on climate change directly by absorbing solar  
67 radiation and indirectly by accelerating snowmelt and affecting the albedo (Qian et al.,  
68 2015; Andreae and Ramanathan, 2013). Based on the remote sensing observations and  
69 chemical transport models (Chung et al., 2012; Wang et al., 2014; Jo et al., 2016), a  
70 non-negligible positive radiative forcing by BrC was found on a global scale with a range  
71 from 0.1 to 0.6 W m<sup>-2</sup>. Beyond that, BrC also influence the atmospheric chemistry and human  
72 health. For example, BrC can shield polycyclic aromatic hydrocarbons (PAHs) from being  
73 oxidized, and thus substantially elevate lung cancer risk from PAHs (Hsu et al., 2014; Yan et  
74 al., 2018).

75 The sources of BrC are complicated, which can be primarily emitted from incomplete  
76 combustion of carbon-containing materials (e.g., biomass, coal and petroleum products.) and  
77 secondarily derived from aqueous-phase reaction (Sun et al., 2017; Gilardoni et al., 2016; Xie  
78 et al., 2018; Nakayama et al., 2013). Biomass burning was found to be a major source of BrC  
79 (Chen and Bond, 2010; Chakrabarty et al., 2010; Saleh et al., 2014), because lignin is of an  
80 unsaturated benzene-like structure, which is a chromophore group. Field measurements and  
81 laboratory studies found that BrC is also secondary sources by forming chromophores during  
82 the atmosphere ageing process, e.g., high-NO<sub>x</sub> photooxidation (Liu et al., 2016; Xie et al.,  
83 2017), ozonolysis of aromatic precursors (Lee et al., 2014), and aqueous-phase photochemical

84 oxidation and polymerization (Smith et al., 2014; Flores et al., 2014; Bones et al., 2010). BrC  
85 products account for very small weight fraction of organic aerosol (OA), but have a  
86 significant effect on OA optical properties. For example, nitroaromatic compounds generated  
87 by photooxidation of toluene under high NO<sub>x</sub> conditions may account for 40-60% of the total  
88 light absorption of toluene-SOA (Lin et al., 2015).

89 Multiple approaches have been developed to quantify the light absorption properties of  
90 BrC (Moosmuller et al., 2009), and a common and sensitive approach is the direct  
91 measurement of spectrophotometric properties of aerosol water or filter extracts by using  
92 optical instrumentation. The advantage of this method can avert interference from insoluble  
93 absorption material (e.g., black carbon) (Cheng et al., 2016; Shen et al., 2017), and supply  
94 high-resolution spectrum over a wide wavelength coverage. Furthermore, it is favorable for  
95 characterization of BrC light-absorbing components by combining with other analytical  
96 techniques, such as mass spectrometry (MS) (Laskin et al., 2015; Corr et al., 2012; Satish et al.,  
97 2017).

98 Many studies have been conducted on the BrC optical properties in China, but most of  
99 those were based on PM<sub>2.5</sub> and PM<sub>10</sub> sample collection and focused on the bulk aerosol  
100 optical properties with no information on the size distributions (Shen et al., 2017; Huang et al.,  
101 2018). Xi'an is a metropolitan city located in Guanzhong Basin of inland China, which is a  
102 typical semiarid region in East Asia and have been suffering from serious particle pollution  
103 due to the large emission of anthropogenic pollutants (Wu et al., 2018; Wang et al., 2016; Wu  
104 et al., 2019), especially intensive coal combustion and biomass burning in winter for house  
105 heating (Wang et al., 2017). In this study, both PM<sub>2.5</sub> and size-segregated aerosol samples in

106 Xi'an were collected during the 2017 winter and summer and analyzed for the characteristics  
107 of BrC. We firstly investigated the seasonal variations of chemical composition and  
108 light-absorption of BrC in the city, then discussed the size distribution of BrC and the impact  
109 of aerosol ageing process on BrC, and finally quantified its source contributions.

## 110 **2. Experimental section**

### 111 **2.1 Sample collection**

112 Aerosol samples were collected on a day/night basis with each for 12-hrs by using a  
113 high-volume ( $\sim 1.13 \text{ m}^3 \text{ min}^{-1}$ ) air sampler (Tisch Environmental, Inc., OH, USA) from  
114 December 31, 2016 to January 22, 2017 (in winter) and from July 18 to August 6, 2017 (in  
115 summer). The sampler was installed on the roof of a three-story building on the campus of the  
116 Institute of Earth Environment, CAS (34.22°N, 108.88°E), which is located at the urban center  
117 of Xi'an, inland China. Meanwhile, size-resolved aerosols with 9 size bins (cutoff points were  
118 0.43, 0.65, 1.1, 2.1, 3.3, 4.7, 5.8, and 9.0  $\mu\text{m}$ , respectively) were collected by using an  
119 Anderson sampler at an airflow rate of  $28.3 \text{ L min}^{-1}$  for 24 hr. All samples were collected onto  
120 the pre-baked ( $450^\circ\text{C}$  for 6 hr) quartz filters and stored in a freezer ( $-18^\circ\text{C}$ ) prior to analysis.

### 121 **2.2 Chemical analysis**

122 A punch ( $0.526 \text{ cm}^3$ ) from each  $\text{PM}_{2.5}$  filter sample was analyzed for organic carbon (OC)  
123 and elemental carbon (EC) with a DRI Model 2001 Thermal/Optical Carbon Analyzer  
124 (Atmoslytic Inc., Calabasas, CA, USA) following the IMPROVE-A protocol (Chow et al.,  
125 2007). More details of the method including quality assurance and quality control (QA/QC)  
126 can be found elsewhere (Wang et al., 2010).

127 Partial filters were cut into pieces, and then extracted three times under sonication with

128 15ml Milli-Q pure water (18.2 MΩ). Ten ions such as  $\text{SO}_4^{2-}$ ,  $\text{NO}_3^-$ ,  $\text{Cl}^-$ ,  $\text{NH}_4^+$ , and  $\text{K}^+$  were  
129 determined using ion chromatography (Dionex, ICS-1100). Similar extraction processes were  
130 also applied to measure the water-soluble organic carbons (WSOC) of the samples, which was  
131 determined by using Shimadzu TOC-5000 Carbon Analyzer. The detailed method has been  
132 reported by Wang et al. (2013). In order to analyze the organic compounds in the samples  
133 such as levoglucosan, PAHs, OPAH and nitrophenols, aliquot of the filter was extracted with a  
134 mixture of methanol and DCM (1:5, v/v), derivatized with BSTFA and measured by using gas  
135 chromatography (HP 7890A, Agilent Co., USA) coupled with mass spectroscopy detector  
136 (GC/MS) (HP 5975, Agilent Co., USA). Details of sample extraction and derivatization were  
137 documented elsewhere (Wang et al., 2009b; Ren et al., 2017). Stable carbon isotope  
138 composition of total carbon ( $\delta^{13}\text{C}_{\text{TC}}$ ) was determined by using an elemental analyzer (EA)  
139 (Carlo Erba, NA 1500) coupled with an isotope ratio mass spectrometer (IRMS, Finnigan  
140 MAT Delta Plus), more details of the method can be referred to elsewhere (Cao et al., 2016).

### 141 **2.3 Light absorption measurements**

142 Brown carbon (BrC) was extracted from a size of  $6\text{ cm}^3$  filter samples for 30min  
143 ultrasonication with 20 ml Milli-Q pure water or methanol. All extracts were then filtered  
144 through  $0.45\ \mu\text{m}$  PTFE (for water) and  $0.22\ \mu\text{m}$  PES (for methanol) pore syringe filter to  
145 remove insoluble components and filter debris. The light-absorption spectra were analyzed  
146 with a UV–visible spectrophotometer (AOE INSTRUMENTS, China) over a wavelength  
147 range of 190–900 nm (Hecobian et al., 2010). The absorption coefficient of water or methanol  
148 extracts ( $\text{M m}^{-1}$ ) could be calculated as the following equation (Teich et al., 2017):

$$\text{abs}_\lambda = (A_\lambda - A_{700}) \frac{V_1}{V_a \times L} \times \ln(10) \quad (1)$$

149 Where  $A_\lambda$  and  $A_{700}$  were the light absorption of the extracts at the wavelength of  $\lambda$  and  
 150 700 nm, respectively.  $V_1$  represented the volume of the solvent extracting the filter sample,  
 151 and  $V_a$  was referred to the volume of air corresponding to the filter punch.  $L$  was the  
 152 absorbing path length (i.e., 1 cm for the currently used quartz cuvettes). The  $\ln(10)$  was  
 153 converted from base 10 (the form provided by the spectrophotometer) to natural logarithms.  
 154 According to the previous studies, the absorption coefficient at 365nm was used as the brown  
 155 carbon absorption in order to avoid disturbance of inorganic salts such as nitrate.

156 The bulk mass absorption coefficient (MAC,  $\text{m}^2/\text{g}$ ) of the extracts at a given wavelength  
 157 can be described by the following equation:

$$\text{MAC} = \frac{\text{abs}_\lambda}{C_{W(M)SOC}} \quad (2)$$

158 Where  $C_{W(M)SOC}$  was the atmospheric concentration of the particulate water-soluble  
 159 (WSOC) or methanol-soluble organic carbon (MSOC,  $\mu\text{gC}/\text{m}^3$ ). In this study, we assumed  
 160 that OC could be completely dissolved in methanol solvent and substituted the MSOC for the  
 161 calculation. This hypothesis would possibly lead to somewhat underestimation of the MAC of  
 162 the methanol extracts, although high extraction efficiency of methanol solvent had been  
 163 reported by previous studies (Liu et al., 2013) .

164 The wavelength dependence of light-absorption with respect to the empirically defined  
 165 power law relationship is described by the following equation (Laskin et al., 2015):

$$\text{MAC} = K\lambda^{-AAE} \quad (3)$$

166 Where  $K$  is a factor that includes aerosol mass concentrations, the AAE is termed as  
167 absorption Angström exponent. In this study, the AAE value of the filter extracts was  
168 determined by a linear regression of  $\log(\text{abs}_\lambda)$  versus  $\log(\lambda)$  over a wavelength range of  
169 300-450nm.

## 170 **2.4 Positive Matrix Factorization (PMF) source apportionment**

171 PMF, as a receptor model, decomposes the sample matrix into two matrices (factor  
172 contributions and factor profiles), and has been widely used for the source apportionment of  
173 atmospheric pollutants. More details on PMF can be found on the EPA website  
174 ([https://www.epa.gov/air-research/epa-positive-matrix-factorization-50-fundamentals-and-use-  
175 r-guide](https://www.epa.gov/air-research/epa-positive-matrix-factorization-50-fundamentals-and-use-r-guide)). In the present work, the mass concentrations of major species (OC, EC, WSOC,  
176  $\text{SO}_4^{2-}$ ,  $\text{NO}_3^-$ ,  $\text{NH}_4^+$ ,  $\text{Ca}^{2+}$ ), organic markers (benzo(b)fluoranthene (BbF), benzo(e)pyrene  
177 (BeP), indeno(1,2,3-c,d)pyrene (IP), levoglucosan, and nitrophenols), and  $\text{abs}_\lambda$  of water extracts  
178 have been used as the input data to perform the source apportionment for brown carbon with  
179 the EPA PMF 5.0 version, similar reports have been found elsewhere (Hecobian et al., 2010).  
180 The model was run numerous times with 3–7 factors and various combinations of the  
181 concentration and absorption data set. Base on the  $Q$  value ( $Q_{\text{true}}$  and  $Q_{\text{robust}}$ ) and  $r$ , which are  
182 indicative of the agreement of the model fit, four factors were obtained as the optimal  
183 solution.

## 184 **3. Results and discussion**

### 185 **3.1 Carbonaceous species in $\text{PM}_{2.5}$ during summer and winter**

186 Figure 1 shows the temporal variations in the concentrations of  $\text{PM}_{2.5}$ , WSOC, OC and  
187  $\text{abs}_{\lambda=365\text{nm}}$  value during the two seasons. WSOC varied from 5.3 to 67  $\mu\text{gC}/\text{m}^3$  in winter with



188 an average of  $23 \pm 13 \mu\text{gC}/\text{m}^3$  (Table 1), which was 4.0 times higher than that in summer. OC  
189 exhibited a similar seasonal variation with WSOC with an average of  $41 \pm 25 \mu\text{gC}/\text{m}^3$  in  
190 winter and  $8.4 \pm 2.4 \mu\text{gC}/\text{m}^3$  in summer, respectively. Whereas, WSOC/OC ratio was much  
191 higher in summer ( $0.70 \pm 0.12$ ) than that in winter ( $0.58 \pm 0.13$ ), partly as a result of an  
192 enhanced photochemical formation of WSOC under the intense sunlight conditions. Similar  
193 phenomena were also found in Beijing (Ping et al., 2017), Shanghai (Zhao et al., 2015a),  
194 Tokyo (Miyazaki et al., 2006) and Southeastern United States (Ding et al., 2008).

195 PAHs, OPAHs, and nitrophenols are ubiquitous in the atmosphere, which can be directed  
196 emitted from incomplete combustion of carbon -containing fuels (e.g., coal, biomass) (Shen et  
197 al., 2013;Zhang and Tao, 2009). In addition, OPAHs and nitrophenols can also be produced  
198 from photochemical reactions (Cochran et al., 2016;Keyte et al., 2013;Yuan et al., 2016).  
199 These compounds are the efficient light-absorbing species, because their molecular structures  
200 consist of chromophores (Lin et al., 2017;Bluvshstein et al., 2017). Herein, 14 PAHs, 7 OPAHs,  
201 and 7 nitrophenols were examined for investigating their effect on BrC absorption. As seen in  
202 Figure S1, the temporal variations of PAHs, OPAHs, and nitrophenols were similar with  
203 levoglucosan, which is the tracer of biomass burning emissions, indicating that biomass  
204 burning is one of the major sources of these compounds. Concentrations of PAHs, OPAHs,  
205 and nitrophenols during winter were  $149 \pm 89 \text{ ng}/\text{m}^3$ ,  $174 \pm 98 \text{ ng}/\text{m}^3$  and  $17 \pm 12 \text{ ng}/\text{m}^3$   
206 (Table 1), respectively, and were 10 - 43 times higher than those in summer, which can be  
207 explained by an increasing emission from residential heating during winter in the city and its  
208 surrounding regions.

209 As shown in Table S1,  $\text{abs}_{\lambda=365\text{nm}}$  extracted by methanol displays showed well correlations

210 with PAHs, OPAHs, and nitrophenols, especially in winter ( $r > 0.89$ ), which suggests that  
211 those species are important light absorption contributors for BrC in Xi'an. Huang et al. (2018)  
212 found that PAHs and OPAHs in Xi'an accounted for, on average, 1.7% of the overall  
213 absorption of methanol-soluble BrC, but their mass fraction in OC was only 0.35%. A recent  
214 study reported that biomass burning also emitted nitroaromatic compounds, particularly  
215 nitrophenols, and accounted for 50-80% of the total visible light absorption ( $> 400$  nm) (Lin  
216 et al., 2017). The robust correlations of above compounds with the absorption at  $\lambda=365$  nm  
217 suggest that PAHs, OPAHs and nitrophenol are strong light-absorbing species.

## 218 **3.2 Light absorption of BrC in water and methanol extracts**

### 219 **3.2.1 Seasonal variations of light absorption by BrC**

220 As shown in Figure 2a and 2b, the marked feature of BrC in Xi'an is that the absorption  
221 spectrum increased notably from the visible to the ultraviolet ranges, and the average  
222  $\text{abs-MeOH}$  at  $\lambda=365$  nm was 1.5 - 1.7 times higher than  $\text{abs-H}_2\text{O}$  in the two seasons,  
223 indicating that MSOC provided a more comprehensive estimation for BrC. Due to enhanced  
224 emission of BrC, average  $\text{abs}_{\lambda=365\text{nm}}$  of BrC found in winter was  $49 \pm 32$  M/m for MeOH and  
225  $28 \pm 16$  M/m for WSOC, which were 9.5- and 8.1-fold higher than that in summer. This  
226 phenomenon was also observed in previous studies in Xi'an (Shen et al., 2017;Huang et al.,  
227 2018) and other areas of China (Du et al., 2014;Chen et al., 2018). Compared with other  
228 regions (Table 2), the absolute  $\text{abs}_{\lambda=365\text{nm}}$  values in Xi'an were slightly lower than that in  
229 Indo-Gangetic Plain, India (Satish et al., 2017;Bachi, 2016), but were considerably higher  
230 than those in Beijing, China (Du et al., 2014), US (Zhang et al., 2011) and Korea (Kim et al.,  
231 2016), suggesting a heavy pollution of light-absorbing aerosols in Xi'an. Furthermore,

232 enhanced  $\text{abs}_{\lambda=365\text{nm}}$  loading in the nighttime was observed during the two seasons, which can  
233 be ascribed to the shallower boundary layer height and the absence of photo-bleaching  
234 processes at night (Saleh et al., 2013;Zhao et al., 2015b).

235 Linear regression slopes on the scatter plots of  $\text{abs}_{\lambda=365\text{nm}}$  values versus WSOC or MSOC  
236 represented the average of MAC at 365 nm (i.e.,  $\text{MAC}_{\text{WSOC}}$  and  $\text{MAC}_{\text{MSOC}}$ ). During winter,  
237 there was a slight disparity between the  $\text{MAC}_{\text{WSOC}}$  and  $\text{MAC}_{\text{MSOC}}$  with the averages of  $1.2 \pm$   
238  $0.06$  and  $1.3 \pm 0.03 \text{ m}^2/\text{g}$  (Figure 2e), respectively, which indicates that there are some similar  
239 chromophores of BrC between the two fractions. As seen in Table 2, both  $\text{MAC}_{\text{WSOC}}$  and  
240  $\text{MAC}_{\text{MSOC}}$  in Xi'an during the two seasons are higher than those in US and Korea, suggesting  
241 that BrC in the city was comprised of stronger light-absorbing compounds.  $\text{abs}_{\lambda=365\text{nm}}$  showed  
242 a strong linear correlation with levoglucosan ( $r > 0.98$ ), suggesting that abundant BrC was  
243 largely derived from biomass burning. As shown in Fig. S2, mass ratios of  
244 levoglucosan/mannosan and levoglucosan/galacosan in the  $\text{PM}_{2.5}$  samples are similar to  
245 biomass types (i.e., woods, leaves, wheat straw), again reflecting that biomass burning  
246 combustion in Xi'an and its surrounding regions are probably the major sources of BrC in the  
247 city during winter. Compared to winter, the MAC in summer was slightly lower, which can be  
248 in part attributed to the less abundant light-absorbing PAHs and OPAHs due to no biomass  
249 burning for house heating. Moreover, with increasing photooxidation in summer,  
250 fragmentation reactions would occur and thus decrease light absorption for BrC aerosols, as  
251 reported by Sumlin et al. (2017), because higher levels of  $\text{O}_3$  and OH radicals in summer  
252 intensify the photooxidation and diminish the BrC aerosol light absorption by reducing the  
253 size of conjugated molecular systems. Interestingly, we found that the  $\text{MAC}_{\text{WSOC}}$  ( $1.1 \pm 0.2$

254  $\text{m}^2/\text{g}$ ) in summer was significantly enhanced compared to  $\text{MAC}_{\text{MSOC}}$  ( $0.8 \pm 0.1 \text{ m}^2/\text{g}$ ), which  
255 can be ascribed to more amount of non-BrC in the methanol extracts such as phthalates, of  
256 which the abundance relative to OC was about 10 time higher in summer than in winter. The  
257  $\text{abs}_{\lambda=365\text{nm}}$  showed a poor correlation with levoglucosan (Table S1), further indicating that the  
258 biomass burning was not the dominant source for BrC in summer.

259 Absorption Ångström exponents (AAE), which were derived from the filter methanol-  
260 and water-extracted BrC ( $\text{AAE}_{\text{WSOC}}$  and  $\text{AAE}_{\text{MSOC}}$ ) for wavelengths between 300 and 450 nm,  
261 were  $6.1 \pm 9.7$  and  $5.3 \pm 8.5$  (Table 2) in winter, respectively, and resembled that in Beijing  
262 (Cheng et al., 2016), Guangzhou (Liu et al., 2018) and Indo- Gangetic Plain (Bachi, 2016),  
263 possibly indicating that the chemical compositions of BrC chromophores in these regions are  
264 similar during winter. As seen in Table 2, unlike those of  $\text{H}_2\text{O}$ -extracts, the averaged values of  
265 MAC and AAE of MeOH extracts were 40% and 10% higher in winter than in summer,  
266 respectively, suggesting that chemical compositions of BrC are different between the two  
267 seasons in the city and the winter BrC contained more non-polar compounds that are of  
268 stronger light-absorbing ability.

### 269 **3.2.2 Aerosol size distribution of BrC**

270 Particles with different sizes are of different chemical compositions, and thus optical  
271 properties of BrC in different size of particles are also different (Zhang et al., 2015;Zhai et al.,  
272 2017). However, information on size distribution of BrC absorption is very limited. In this  
273 study, we mainly focused on the water-extracted samples, because particles deposited on the  
274 filter surface are unevenly distributed, making the quantifications of OC and EC in the  
275 size-segregated samples not accurate enough. As shown in Figure S3, there was a good

276 relationship between the  $\text{abs}_{\lambda=365\text{nm}}$  ( $r > 0.98$ ) of the samples collected by Anderson sampler  
277 and those collected by high-volume  $\text{PM}_{2.5}$  sampler (Fig. S3), suggesting a good agreement  
278 between the two sampling methods.

279 As show in Figure 3,  $\text{abs}_{\lambda=365\text{nm}}$  presented a bimodal pattern during winter and summer,  
280 dominating at the fine mode ( $D_p < 2.1\mu\text{m}$ ) with relative contributions of 81% and 65% to the  
281 total absorption in the two seasons, respectively. These proportions are similar to those  
282 reported for a forest wildfire event, which showed that 93% of the total BrC absorption was in  
283 the fine particles ( $0.10 < D_p < 1.0\mu\text{m}$ ) (Lorenzo et al., 2018). Maximum absorptions were  
284 observed at 1.02 and  $0.71\mu\text{m}$  ( $D_{pg}$ - geometric mean diameters, Figure 3a and 3b) in winter  
285 and summer, respectively, which is in agreement with the observations by Lei et al (2018),  
286 who found that the major peaks for BrC absorption were in the rang from  $0.5\mu\text{m}$  to  $1.0\mu\text{m}$  in  
287 urban and may shift toward smaller size ( $< 0.4\mu\text{m}$ ) for particles released from burning  
288 experiments (Lei et al., 2018). However, the size distribution pattern of MAC was different  
289 from that of  $\text{abs}_{\lambda=365\text{nm}}$  in Xi'an, which presented a monomodal distribution with a peak in the  
290 fine mode ( $< 2.1\mu\text{m}$ ) in winter and a bimodal distribution in summer with two peaks in the fine  
291 ( $< 2.1\mu\text{m}$ ) and coarse ( $> 2.1\mu\text{m}$ ) modes, respectively (Figure 3c and 3d). As seen in Figure 3c  
292 and 3d, the fine mode of MAC was around 50% larger in winter than that in summer,  
293 suggesting that water-soluble fraction of winter fine particles was more light-absorbing  
294 compared to that in summer, probably due to the summertime stronger bleaching effect.

### 295 **3.3 Underestimation of BrC absorption by solvent extraction methods**

296 A few studies pointed out that absorption properties of BrC extracted by bulk solution  
297 may not entirely reflect the light absorption by ambient aerosols. Here, we further calculated

298 the light absorption of the samples using the Mie theory combined with an imaginary ( $k$ ,  
299 responsible for absorption) refractive index with assumptions that particles were of spherical  
300 morphology and externally mixed with other light-absorbing components. The imaginary  
301 refractive index could be obtained from MAC using follow equation (Laskin et al., 2015):

$$k_{(\lambda)} = \frac{\rho \lambda \text{ abs}}{4\pi \times \text{WSOC}} = \frac{\rho \lambda \text{ MAC}}{4\pi} \quad (4)$$

302 Where  $\rho$  ( $\text{g/cm}^3$ ) was particle density and assigned as 1.5, more details about Mie  
303 calculations can be referred to the study by Liu et al. (2013).

304 As noted above, most BrC aerosols were in the fine mode ( $<2.1\mu\text{m}$ ), thus, here we only  
305 focused on this fraction for the Mie calculations. The values of imaginary refractive in winter  
306 remains nearly constant (0.038-0.048) for different particle sizes at  $\lambda=365$  nm (Table 3),  
307 which was about two times smaller than that ( $0.093 \pm 0.049$ ) over Gangetic Plain, India  
308 (Shamjad et al., 2017). Values of  $k$  in summer were slight smaller when compared to those in  
309 winter, suggesting that the aerosols in summer were more aged. Sumlin et al. (2017) found  
310 that  $k$  decreases along with the atmospheric aging from  $0.029 \pm 0.001$  to  $0.019 \pm 0.001$  at  
311  $\lambda=375$  nm. However,  $k$  values in this study were 5.0 times (avg.) higher than those reported  
312 from the United States (Liu et al., 2013). This is because that  $\text{PM}_{2.5}$  particles in Xi'an, China  
313 are enriched in BrC and the mass absorption coefficient was considerably higher than that in  
314 US. Figure 4 compares the difference between  $\text{abs}_{\lambda=365\text{nm}}$  predicted by Mie theory (abs-Mie)  
315 and that extracted by the bulk solution (abs-Measure). Mie theory predicted  $\text{abs}_{\lambda=365\text{nm}}$  was  
316 1.5-fold higher than that measured by the bulk solution, suggesting that the solvent extraction  
317 methods, which have commonly been used for atmospheric BrC measurements, could result

318 in an underestimation on optical absorption of aerosols. Hence, a factor of 1.5 is  
319 recommended to convert the liquid-based data (at least for the water-soluble data) reported by  
320 this work for estimating optical properties of atmospheric aerosols in Xi'an and its  
321 surrounding regions in order to better quantify the BrC light-absorption.

### 322 **3.4 The characteristic of BrC with the aerosol aging**

323 During the ageing process, secondary organic aerosols (SOA) with strong chromophores  
324 can be generated and efficiently absorb solar radiation (Lin et al., 2014; Lin et al., 2016). From  
325 Figure 5, it can be found that air quality in Xi'an during the winter varied from the clean  
326 ( $PM_{2.5} < 75 \mu\text{g}/\text{m}^3$ ) to the polluted conditions ( $PM_{2.5} > 75 \mu\text{g}/\text{m}^3$ ) from the period of 12<sup>th</sup>  
327 January to 19<sup>th</sup> January. Such a case provides an opportunity to investigate the changes in  
328 light-absorption by BrC during the aerosol ageing process.

329 As shown in Figure 5a and 5b,  $ab_{S\lambda=365\text{nm}}$  extracted by water and MeOH in Xi'an during  
330 the campaign showed an increasing trend from 12<sup>th</sup> January to 19<sup>th</sup> January, which is similar  
331 to  $PM_{2.5}$  loadings but opposite to the visibility, indicating that BrC is one of the important  
332 factors leading to the visibility deterioration. From Figure 5b, it can also be seen that light  
333 absorption of water-extracts dominated over the total BrC absorption especially in daytime  
334 and showed a variation pattern similar to the  $PM_{2.5}$  (Figure 5a) and WSOC loadings (Figure  
335 5c), indicating a continuous formation of secondary BrC during the aerosol ageing process. To  
336 illustrate this point, the stable carbon isotopic composition ( $\delta^{13}\text{C}_{\text{TC}}$ ) of total carbon (TC) in the  
337 samples was measured. WSOC/OC showed a positive correlation with the  $\delta^{13}\text{C}_{\text{TC}}$ ,  
338 demonstrating an ageing process of aerosols during the haze development from 12<sup>th</sup> to 19<sup>th</sup>,  
339 January, although it was weak ( $r = 0.47$ ,  $n = 17$ ). Similar conclusions were also reported by

340 Yang et al. (2004) and Pavuluri et al. (2015). From Figure 5c, increasing trends of OPAHs and  
341 nitrophenols were observed during the haze development, suggesting that more SOAs with  
342 chromophores were generated during such an aerosol ageing process, because these  
343 compounds are also of secondary origins. To exclude the possible impact of the changes in  
344 BrC source emissions, the values of PAHs/OC and levoglucosan/OC were applied in this study,  
345 because PAHs and levoglucosan emission factors are different for different  
346 sources (Nguyen-Duy and Chang, 2017). As shown in Fig. S4, both values indistinctively  
347 changed during the aerosol ageing process, indicating that the increasing  $abs_{\lambda=365nm}$  were not  
348 caused by the changes in source emissions. Moreover, we found that  $MAC_{MSOC}$  values during  
349 the age process also increased (Figure 5a), further suggesting that the bleaching effect on  
350 light-absorbing BrC was reducing during the haze developing process.

351 EC is one of the major light-absorbing aerosols in the atmosphere (Collier et al.,  
352 2018; Peng et al., 2016). To further discuss the changes of BrC during the aerosol ageing  
353 process, we compared the mass absorption efficiency of EC at  $\lambda=550\text{ nm}$  ( $7.5 \pm 1.2\text{ m}^2/\text{g}$ )  
354 with BrC by using the method reported from Yan et al. (2015) and Kirillova et al. (2014). As  
355 shown in Figure 5c, the concentrations of EC have a slight change in the haze period, so the  
356 changes in light absorption of EC remained nearly constant. However, the ratio of  
357  $abs_{\lambda=365nm}\text{-MeOH}/abs_{\lambda=550nm}\text{-EC}$  increasingly became larger along with the visibility  
358 deterioration from January 12<sup>th</sup> to January 19<sup>th</sup> (Fig. 5b), while the mass ratios of PAHs/EC,  
359 OPAHs/EC and nitrophenols /EC during the period showed a significant negative correlation  
360 with visibility (Fig. S5), further suggesting that the impairment of BrC on the visibility was  
361 getting more significant during the haze development process.



362 During the haze developing process, organic aerosols are usually getting more aged and  
363 enriched in heavier  $^{13}\text{C}$  due to the kinetic isotopic effect (KIE) (Wang et al., 2010). As shown  
364 in Figure 6a and b,  $\delta^{13}\text{C}$  of  $\text{PM}_{2.5}$  samples presented a strong positive correlation with  $\text{abs}_{\lambda=365}$   
365  $\text{nm-MeOH}$  ( $r=0.82$ ) in the daytime, while there was no such a correlation in the nighttime  
366 during the haze period of January 12<sup>th</sup> -19<sup>th</sup>, indicating a daytime formation of secondary BrC.  
367 From Figure 6c and 6d, we also found that the correlation of  $\text{abs}_{\lambda=365 \text{ nm-MeOH}} / \text{abs}_{\lambda=550 \text{ nm-EC}}$   
368 ratio with nitrophenol was much stronger in daytime than in nighttime, which is opposite to  
369 the correlation of  $\text{abs}_{\lambda=365 \text{ nm-MeOH}} / \text{abs}_{\lambda=550 \text{ nm-EC}}$  ratio with PAHs. Nitrophenols can be  
370 produced from secondary photooxidation of phenol with  $\text{NO}_x$ , while PAHs are produced  
371 solely from direct emissions especially from coal and biomass burning for house heating. The  
372 opposite diurnal correlations of  $\text{abs}_{\lambda=365 \text{ nm-MeOH}} / \text{abs}_{\lambda=550 \text{ nm-EC}}$  ratio with nitrophenols and  
373 PAHs again revealed an enhanced formation of secondary BrC during the aerosol ageing  
374 process.

### 375 **3.5 Positive matrix factorization (PMF) analysis for BrC source apportionment**

376 In the current work, The EPA PMF 5.0 model was used for identifying the possible  
377 sources of BrC. Because the number of the collected samples in each season was not large  
378 enough, data from the two seasons were merged together to form a dataset of  $80 \times 12$  (80  
379 samples with 12 species) in order to obtain an accurate analysis according to the PMF user  
380 guide. The resolved source profiles (factors) represented the sources that influenced  
381 variability in the selected components throughout two seasons in Xi'an. Similar approach was  
382 also reported by Zhang et al. (2010). With several iterative testes, a solution with four factors  
383 was identified as the optimal solution. As shown in Table S2, the values of  $Q_{\text{true}}$  and  $Q_{\text{robust}}$

384 were consistent, which indicates that the model fits the input data well. Furthermore, the  
385 correlation coefficient between input and model values ranged from 0.82 to 0.99 with an  
386 average 0.96, also implying that the model fit well. This assess method was widely used in  
387 previous studies (Ren et al., 2017;Wang et al., 2009a).

388 Figure7 shows the factor profiles resolved by the model. Factor 01 was characterized by  
389 high levels of BeF (52%), BeP (57%), and IP (67%), which were primarily derived from coal  
390 combustion and vehicle exhausts (Kong et al., 2010;Ma et al., 2010;Harrison et al., 1996),  
391 further, relatively high OC (29%) and EC (25%) associated with this factor was well known  
392 tracers of exhaust emissions (Zong et al., 2016), so we identified Factor 01as the source from  
393 fossil fuel combustion. Factor 02 (fugitive dust) shows high contribution of Ca<sup>2+</sup> (69%) and a  
394 moderate loading of EC (39%). Ca, as one of the most abundant crustal elements, is largely  
395 from construction work, resuspended dust or soil sources (Chow et al., 2004;Han et al., 2007).  
396 In addition, EC was a well-known tracer of vehicular emissions (Dorado et al., 2003), so this  
397 factor can be attributed to the impact of vehicles passing with higher speeds, leading to  
398 resuspend non-tailpipe particles. Moreover, the concentrations of Ca<sup>2+</sup> in the night were  
399 almost higher than that during the day time, with averages of  $1.8 \pm 1.56$  and  $1.43 \pm 0.85 \mu\text{g}/\text{m}^3$ ,  
400 respectively. This is consistent with time for transporting the construction wastes by lorry.  
401 Thus, factor 02 was identified as fugitive dust. Factor 03 was identified as secondary  
402 formation, as it is associated with high loadings of NO<sub>3</sub><sup>-</sup> (63%), SO<sub>4</sub><sup>2-</sup> (73%), NH<sub>4</sub><sup>+</sup> (69%) and  
403 a moderate loading of OC and WSOC, indicating the presence of secondary inorganic and  
404 organic aerosols. The factor 04 showed high loadings with nitrophenols, levoglucosan, and  
405 abs-MeOH and was identified as biomass burning, because levoglucosan is the tracer for

406 biomass burning smoke, and nitrophenols can be produced in the aging process of biomass  
407 burning plume.

408 Figure 8 shows the contributions of the above sources to the light absorption at  $\lambda=365\text{nm}$ ,  
409 which also represents the fraction of BrC for the factors. Biomass burning was the primary  
410 source of the BrC, accounting for 55% of the total BrC in the city, which is coincided with the  
411 results discussed in the section 3.2.1. A significant fraction (about 19%) of BrC was  
412 associated with fossil fuel combustion. The fraction of secondary BrC was about 16%, which  
413 was enhanced during the summer due to the efficient photochemical formation of secondary  
414 chromophores. The AAE value of total BrC, closed to the aged SOA-AAE (4.7-5.3) (Bones et  
415 al., 2010), can also verify it. The remaining fraction of BrC was derived from the fugitive dust  
416 in the city. The results of BrC source apportionment for the Xi'an samples are in line with the  
417 work by Shen et al. (2017) and also similar to the results obtained in Beijing by using  
418 radiocarbon fingerprinting (Yan et al., 2017).

#### 419 **4. Conclusions**

420 This study investigated the seasonality of the light-absorption characteristics of BrC in  
421 Xi'an. Light absorption coefficient (MAC) of methanol-extracts at 365nm was 1.5-1.7 folds  
422 higher than that of water-extracts in the two seasons, suggesting non-polar compounds in the  
423 city are of stronger light-absorbing ability than that of polar compounds. The strong  
424 correlation of levoglucosan with BrC and the diagnostic ratios of levoglucosan/mannosan and  
425 levoglucosan/galacosan revealed that the wintertime abundant BrC ( $\text{abs}_{\lambda=365\text{nm}}\text{-MeOH}$  of  
426  $49.18 \pm 31.67 \text{ M/m}$ ) in Xi'an was mainly derived from the residential biofuel combustion for  
427 house heating in the city and its surrounding region. Size distribution results showed that 81%

428 and 65% of BrC occurred in the fine mode ( $< 2.1\mu\text{m}$ ) during winter and summer, respectively,  
429 which is characterized by a monomodal size distribution with a peak in winter and a bimodal  
430 size distribution in summer with two peaks in the fine and coarse modes, respectively. The  
431 fine mode of MAC is 50% higher in winter than that in summer, suggesting that the  
432 light-absorbing ability of wintertime fine particles is stronger, due to the abundant occurrence  
433 of PAHs and other aromatic compounds in the fine mode.

434 The linear correlation between the ratio of  $\text{abs}_{\lambda=365\text{nm}}\text{-MeOHO}/\text{abs}_{\lambda=550\text{nm}}\text{-EC}$  and the  
435 enrichment of  $^{13}\text{C}$  during the haze development indicated an accumulation of secondary BrC  
436 in the aerosol ageing process. The daytime strong correlation of the ratio of  
437  $\text{abs}_{\lambda=365\text{nm}}\text{-MeOHO}/\text{abs}_{\lambda=550\text{nm}}\text{-EC}$  with nitrophenols in the haze event further revealed that  
438 such an enhanced production of secondary BrC is related to the photooxidation of aromatic  
439 compounds with  $\text{NO}_x$ . Source apportionment by using PMF showed that 55% of the BrC was  
440 associated with biomass burning in the city during the campaign, with 19 and 16% of BrC  
441 derived from fossil fuel combustion and secondary formation, respectively.

442  
443  
444

445 Author contributions. GW designed the experiment. CW, JianjunL, JinL and CC collected the  
446 samples. CW and ZZ conducted the experiments. CW and GW performed the data  
447 interpretation and wrote the paper. All authors contributed to the paper with useful scientific  
448 discussions or comments.

449  
450  
451

452 Competing interests. The authors declare that they have no conflict of interest.

453  
454  
455  
456

457 Acknowledgements. This work was financially supported by National Key R&D Plan  
458 (Quantitative Relationship and Regulation Principle between Regional Oxidation Capacity of  
459 Atmospheric and Air Quality (No. 2017YFC0210000), the program from National Nature  
460 Science Foundation of China (No. 41773117).

## 461 **References**

- 462 Andreae, M. O., and Ramanathan, V.: Climate change. Climate's dark forcings, *Science*, 340, 280-281,  
463 10.1126/science.1235731, 2013.
- 464 Bachi, S.: Mass absorption efficiency of light absorbing organic aerosols from source region of paddy-residue  
465 burning emissions in the Indo-Gangetic Plain, *Atmospheric Environment*, 125, 360-370,  
466 10.1016/j.atmosenv.2015.07.017, 2016.
- 467 Bluvshstein, N., Lin, P., Flores, J. M., Segev, L., Mazar, Y., Tas, E., Snider, G., Weagle, C., Brown, S. S., and  
468 Laskin, A.: Broadband optical properties of biomass burning aerosol and identification of brown carbon  
469 chromophores, *Journal of Geophysical Research*, 122, 10.1002/2016JD026230, 2017.
- 470 Bones, D. L., Henricksen, D. K., Mang, S. A., Gonsior, M., Bateman, A. P., Nguyen, T. B., Cooper, W. J., and  
471 Nizkorodov, S. A.: Appearance of strong absorbers and fluorophores in limonene-O<sub>3</sub>secondary organic  
472 aerosol due to NH<sub>4</sub><sup>+</sup>-mediated chemical aging over long time scales, *Journal of Geophysical Research*, 115,  
473 10.1029/2009jd012864, 2010.
- 474 Cao, F., Zhang, S.-C., Kawamura, K., and Zhang, Y.-L.: Inorganic markers, carbonaceous components and stable  
475 carbon isotope from biomass burning aerosols in Northeast China, *Science of the Total Environment*, 572,  
476 1244-1251, 10.1016/j.scitotenv.2015.09.099, 2016.
- 477 Chakrabarty, R. K., Moosmüller, H., Chen, L. W. A., and Lewis, K.: Brown carbon in tar balls from smoldering  
478 biomass combustion, *Atmospheric Chemistry and Physics*, 10, 6363-6370, 10.5194/acp-10-6363-2010,  
479 2010.
- 480 Chen, Y., and Bond, T. C.: Light absorption by organic carbon from wood combustion, *Atmospheric Chemistry  
481 & Physics Discussions*, 9, 1773-1787, 10.5194/acp-10-1773-2010, 2010.
- 482 Chen, Y., Ge, X., Chen, H., Xie, X., Chen, Y., Wang, J., Ye, Z., Bao, M., Zhang, Y., and Chen, M.: Seasonal light  
483 absorption properties of water-soluble brown carbon in atmospheric fine particles in Nanjing, China,  
484 *Atmospheric Environment*, 230-240, 10.1016/j.atmosenv.2018.06.002, 2018.
- 485 Cheng, Y., He, K. B., Du, Z. Y., Engling, G., Liu, J. M., Ma, Y. L., Zheng, M., and Weber, R. J.: The  
486 characteristics of brown carbon aerosol during winter in Beijing, *Atmospheric Environment*, 127, 355-364,  
487 10.1016/j.atmosenv.2015.12.035, 2016.
- 488 Chow, J. C., Watson, J. G., Kuhns, H., Etyemezian, V., Lowenthal, D. H., Crow, D., Kohl, S. D., Engelbrecht, J.  
489 P., and Green, M. C.: Source profiles for industrial, mobile, and area sources in the Big Bend Regional  
490 Aerosol Visibility and Observational study, *Chemosphere*, 54, 185-208,  
491 10.1016/j.chemosphere.2003.07.004, 2004.
- 492 Chow, J. C., Watson, J. G., Chen, L. W., Chang, M. C., Robinson, N. F., Trimble, D., and Kohl, S.: The  
493 IMPROVE\_A temperature protocol for thermal/optical carbon analysis: maintaining consistency with a  
494 long-term database, *Journal of the Air & Waste Management Association*, 57, 1014-1023,  
495 10.3155/1047-3289.57.9.1014, 2007.
- 496 Chung, C. E., Ramanathan, V., and Decremier, D.: Observationally-constrained Estimates of Carbonaceous  
497 Aerosol Radiative Forcing, *PROCEEDINGS OF THE NATIONAL ACADEMY OF SCIENCES OF THE*

498 UNITED STATES OF AMERICA, 109, 11624-11629, 10.1073/pnas.1203707109, 2012.

499 Cochran, R. E., Jeong, H., Haddadi, S., Fisseha Derseh, R., Gowan, A., Beránek, J., and Kubátová, A.:  
500 Identification of products formed during the heterogeneous nitration and ozonation of polycyclic aromatic  
501 hydrocarbons, *Atmospheric Environment*, 128, 92-103, 10.1016/j.atmosenv.2015.12.036, 2016.

502 Collier, S., Williams, L. R., Onasch, T. B., Cappa, C. D., Zhang, X., Russell, L. M., Chen, C.-L., Sanchez, K. J.,  
503 Worsnop, D. R., and Zhang, Q.: Influence of Emissions and Aqueous Processing on Particles Containing  
504 Black Carbon in a Polluted Urban Environment: Insights From a Soot Particle-Aerosol Mass Spectrometer,  
505 *Journal of Geophysical Research-Atmospheres*, 123, 6648-6666, 10.1002/2017jd027851, 2018.

506 Corr, C. A., Hall, S. R., Ullmann, K., and Anderson, B. E.: Spectral absorption of biomass burning aerosol  
507 determined from retrieved single scattering albedo during ARCTAS, *Atmospheric Chemistry and Physics*,  
508 12, 10505-10518, 10.5194/acp-12-10505-2012, 2012.

509 Ding, X., Zheng, M., Yu, L., Zhang, X., Weber, R. J., Yan, B., Russell, A. G., Edgerton, E. S., and Wang, X.:  
510 Spatial and Seasonal Trends in Biogenic Secondary Organic Aerosol Tracers and Water-Soluble Organic  
511 Carbon in the Southeastern United States, *Environmental Science & Technology*, 42, 5171-5176,  
512 10.1021/es7032636, 2008.

513 Dorado, M. P., Ballesteros, E., Arnal, J. M., Gómez, J., and López, F. J.: Exhaust emissions from a Diesel engine  
514 fueled with transesterified waste olive oil ☆, *Fuel*, 82, 1311-1315, 10.1016/S0016-2361(03)00034-6, 2003.

515 Du, Z., He, K., Cheng, Y., Duan, F., Ma, Y., Liu, J., Zhang, X., Zheng, M., and Weber, R.: A yearlong study of  
516 water-soluble organic carbon in Beijing II: Light absorption properties, *Atmospheric Environment*, 89,  
517 235-241, 10.1016/j.atmosenv.2014.02.022, 2014.

518 Flores, J. M., Washenfelder, R. A., Adler, G., Lee, H. J., Segev, L., Laskin, J., Laskin, A., Nizkorodov, S. A.,  
519 Brown, S. S., and Rudich, Y.: Complex refractive indices in the near-ultraviolet spectral region of biogenic  
520 secondary organic aerosol aged with ammonia, *Physical Chemistry Chemical Physics*, 16, 10629-10642,  
521 10.1039/c4cp01009d, 2014.

522 Gilardoni, S., Massoli, P., Paglione, M., Giulianelli, L., Carbone, C., Rinaldi, M., Decesari, S., Sandrini, S.,  
523 Costabile, F., Gobbi, G. P., Pietrogrande, M. C., Visentin, M., Scotto, F., Fuzzi, S., and Facchini, M. C.:  
524 Direct observation of aqueous secondary organic aerosol from biomass-burning emissions, *Proceedings of  
525 the National Academy of Sciences of the United States of America*, 113, 10013-10018,  
526 10.1073/pnas.1602212113, 2016.

527 Gustafsson, O., Kruså, M., Zencak, Z., Sheesley, R. J., Granat, L., Engström, E., Praveen, P. S., Rao, P. S., Leck,  
528 C., and Rodhe, H.: Brown clouds over South Asia: biomass or fossil fuel combustion?, *Science*, 323,  
529 495-498, 10.1126/science.1164857, 2009.

530 Han, L., Zhuang, G., Cheng, S., Wang, Y., and Li, J.: Characteristics of re-suspended road dust and its impact on  
531 the atmospheric environment in Beijing, *Atmospheric Environment*, 41, 7485-7499,  
532 10.1016/j.atmosenv.2007.05.044, 2007.

533 Harrison, R. M., Smith, D. J. T., and Luhana, L.: Source Apportionment of Atmospheric Polycyclic Aromatic  
534 Hydrocarbons Collected from an Urban Location in Birmingham, U.K, *Environmental Science &  
535 Technology*, 30, 825-832, 10.1021/es950252d, 1996.

536 Hecobian, A., Zhang, X., Zheng, M., Frank, N., Edgerton, E. S., and Weber, R. J.: Water-Soluble Organic  
537 Aerosol material and the light-absorption characteristics of aqueous extracts measured over the  
538 Southeastern United States, *Atmospheric Chemistry and Physics*, 10, 5965-5977,  
539 10.5194/acp-10-5965-2010, 2010.

540 Hsu, H. I., Lin, M. Y., Chen, Y. C., Chen, W. Y., Yoon, C., Chen, M. R., and Tsai, P. J.: An integrated approach to

541 assess exposure and health-risk from polycyclic aromatic hydrocarbons (PAHs) in a fastener manufacturing  
542 industry, *International Journal of Environmental Research & Public Health*, 11, 9578-9594,  
543 10.3390/ijerph110909578, 2014.

544 Huang, R. J., Yang, L., Cao, J., Chen, Y., Chen, Q., Li, Y., Duan, J., Zhu, C., Dai, W., and Wang, K.: Brown  
545 Carbon Aerosol in Urban Xi'an, Northwest China: The Composition and Light Absorption Properties,  
546 *Environmental Science & Technology*, 52, 6825-6833 10.1021/acs.est.8b02386, 2018.

547 Jo, D. S., Park, R. J., Lee, S., Kim, S. W., and Zhang, X. L.: A global simulation of brown carbon: implications  
548 for photochemistry and direct radiative effect, *Atmospheric Chemistry and Physics*, 16, 3413-3432,  
549 10.5194/acp-16-3413-2016, 2016.

550 Keyte, I. J., Harrison, R. M., and Lammel, G.: Chemical reactivity and long-range transport potential of  
551 polycyclic aromatic hydrocarbons - a review, *Chemical Society Reviews*, 42, 9333-9391,  
552 10.1039/c3cs60147a, 2013.

553 Kim, H., Jin, Y. K., Jin, H. C., Ji, Y. L., and Lee, S. P.: Seasonal variations in the light-absorbing properties of  
554 water-soluble and insoluble organic aerosols in Seoul, Korea, *Atmospheric Environment*, 129, 234-242,  
555 10.1016/j.atmosenv.2016.01.042, 2016.

556 Kirillova, E. N., Andersson, A., Tiwari, S., Srivastava, A. K., Bisht, D. S., and Öörjan, G.: Water-soluble organic  
557 carbon aerosols during a full New Delhi winter: Isotope-based source apportionment and optical properties,  
558 *Journal of Geophysical Research Atmospheres*, 119, 3476-3485, 10.1002/2013JD020041, 2014.

559 Kong, S., Ding, X., Bai, Z., Han, B., Chen, L., Shi, J., and Li, Z.: A seasonal study of polycyclic aromatic  
560 hydrocarbons in PM(2.5) and PM(2.5-10) in five typical cities of Liaoning Province, China, *J Hazard Mater*,  
561 183, 70-80, 10.1016/j.jhazmat.2010.06.107, 2010.

562 Laskin, A., Laskin, J., and Nizkorodov, S. A.: Chemistry of atmospheric brown carbon, *Chem Rev*, 115,  
563 4335-4382, 10.1021/cr5006167, 2015.

564 Lee, H. J., Aiona, P. K., Laskin, A., Laskin, J., and Nizkorodov, S. A.: Effect of solar radiation on the optical  
565 properties and molecular composition of laboratory proxies of atmospheric brown carbon, *Environmental  
566 Science & Technology*, 48, 10217-10226, 10.1021/es502515r, 2014.

567 Lei, Y., Shen, Z., Zhang, T., Zhang, Q., Wang, Q., Sun, J., Gong, X., Cao, J., Xu, H., and Liu, S.: Optical source  
568 profiles of brown carbon in size-resolved particulate matter from typical domestic biofuel burning over  
569 Guanzhong Plain, China, *Science of the Total Environment*, 622, 244-251, 10.1016/j.scitotenv.2017.11.353,  
570 2018.

571 Lin, G., Penner, J. E., Flanner, M. G., Sillman, S., Xu, L., and Zhou, C.: Radiative forcing of organic aerosol in  
572 the atmosphere and on snow: Effects of SOA and brown carbon, *Journal of Geophysical Research:  
573 Atmospheres*, 119, 7453-7476, 10.1002/2013jd021186, 2014.

574 Lin, P., Liu, J., Shilling, J. E., Kathmann, S. M., Laskin, J., and Laskin, A.: Molecular characterization of brown  
575 carbon (BrC) chromophores in secondary organic aerosol generated from photo-oxidation of toluene, *Phys  
576 Chem Chem Phys*, 17, 23312-23325, 10.1039/c5cp02563j, 2015.

577 Lin, P., Aiona, P. K., Li, Y., Shiraiwa, M., Laskin, J., Nizkorodov, S. A., and Laskin, A.: Molecular  
578 Characterization of Brown Carbon in Biomass Burning Aerosol Particles, *Environmental Science &  
579 Technology*, 50, 11815-11824, 10.1021/acs.est.6b03024, 2016.

580 Lin, P., Bluvshstein, N., Rudich, Y., Nizkorodov, S. A., Laskin, J., and Laskin, A.: Molecular Chemistry of  
581 Atmospheric Brown Carbon Inferred from a Nationwide Biomass Burning Event, *Environmental Science &  
582 Technology*, 51, 11561-11570, 10.1021/acs.est.7b02276, 2017.

583 Liu, J., Bergin, M., Guo, H., King, L., Kotra, N., Edgerton, E., and Weber, R. J.: Size-resolved measurements of

584 brown carbon in water and methanol extracts and estimates of their contribution to ambient fine-particle  
585 light absorption, *Atmospheric Chemistry and Physics*, 13, 12389-12404, 10.5194/acp-13-12389-2013, 2013.

586 Liu, J., Lin, P., Laskin, A., Laskin, J., Kathmann, S. M., Wise, M., Caylor, R., Imholt, F., Selimovic, V., and  
587 Shilling, J. E.: Optical properties and aging of light-absorbing secondary organic aerosol, *Atmospheric*  
588 *Chemistry & Physics*, 16, 1-36, 2016.

589 Liu, J., Mo, Y., Ding, P., Li, J., Shen, C., and Zhang, G.: Dual carbon isotopes ( $(^{14}\text{C})$  and  $(^{13}\text{C})$ ) and optical  
590 properties of WSOC and HULIS-C during winter in Guangzhou, China, *Sci Total Environ*, 633, 1571-1578,  
591 10.1016/j.scitotenv.2018.03.293, 2018.

592 Lorenzo, R. D., Place, B. K., Vandenboer, T. C., and Young, C. J.: Composition of Size-Resolved Aged Boreal  
593 Fire Aerosols: Brown Carbon, Biomass Burning Tracers, and Reduced Nitrogen, *ACS Earth and Space*  
594 *Chemistry*, 2, 278-285, 10.1021/acsearthspacechem.7b00137, 2018.

595 Ma, W. L., Li, Y. F., Qi, H., Sun, D. Z., Liu, L. Y., and Wang, D. G.: Seasonal variations of sources of polycyclic  
596 aromatic hydrocarbons (PAHs) to a northeastern urban city, China, *Chemosphere*, 79, 441-447,  
597 10.1016/j.chemosphere.2010.01.048, 2010.

598 Miyazaki, Y., Kondo, Y., Takegawa, N., Komazaki, Y., Fukuda, M., Kawamura, K., Mochida, M., Okuzawa, K.,  
599 and Weber, R. J.: Time-resolved measurements of water-soluble organic carbon in Tokyo, *Journal of*  
600 *Geophysical Research Atmospheres*, 111, -, 10.1029/2006JD007125, 2006.

601 Moosmuller, H., Chakrabarty, R. K., and Arnott, W. P.: Aerosol light absorption and its measurement: A review, *J.*  
602 *Quant. Spectrosc. Radiat. Transf.*, 110, 844-878, 10.1016/j.jqsrt.2009.02.035, 2009.

603 Nakayama, T., Sato, K., Matsumi, Y., Imamura, T., Yamazaki, A., and Uchiyama, A.: Wavelength and NO<sub>x</sub>  
604 dependent complex refractive index of SOAs generated from the photooxidation of toluene, *Atmospheric*  
605 *Chemistry and Physics*, 13, 531-545, 10.5194/acp-13-531-2013, 2013.

606 Nguyen-Duy, D., and Chang, M. B.: Review on characteristics of PAHs in atmosphere, anthropogenic sources  
607 and control technologies, *Science of the Total Environment*, 609, 682-693, 10.1016/j.scitotenv.2017.07.204,  
608 2017.

609 Pavuluri, C. M., Kawamura, K., and Swaminathan, T.: Time-resolved distributions of bulk parameters, diacids,  
610 ketoacids and  $\alpha$ -dicarbonyls and stable carbon and nitrogen isotope ratios of TC and TN in tropical Indian  
611 aerosols: Influence of land/sea breeze and secondary processes, *Atmospheric Research*, 153, 188-199,  
612 10.1016/j.atmosres.2014.08.011, 2015.

613 Peng, J., Hu, M., Guo, S., Du, Z., Zheng, J., Shang, D., Zamora, M. L., Zeng, L., Shao, M., Wu, Y.-S., Zheng, J.,  
614 Wang, Y., Glen, C. R., Collins, D. R., Molina, M. J., and Zhang, R.: Markedly enhanced absorption and  
615 direct radiative forcing of black carbon under polluted urban environments, *Proceedings of the National*  
616 *Academy of Sciences of the United States of America*, 113, 4266-4271, 10.1073/pnas.1602310113, 2016.

617 Ping, X., Zhou, X., Duan, J., Tan, J., He, K., Yuan, C., Ma, Y., and Zhang, Y.: Chemical characteristics of  
618 water-soluble organic compounds (WSOC) in PM 2.5 in Beijing, China: 2011–2012, *Atmospheric Research*,  
619 183, 104-112, 10.1016/j.atmosres.2016.08.020, 2017.

620 Qian, Y., Yasunari, T. J., Doherty, S. J., Flanner, M. G., Lau, W. K. M., Ming, J., Wang, H., Wang, M., Warren, S.  
621 G., and Zhang, R.: Light-absorbing particles in snow and ice: Measurement and modeling of climatic and  
622 hydrological impact, *Advances in Atmospheric Sciences*, 32, 64-91, 10.1007/s00376-014-0010-0, 2015.

623 Ren, Y., Wang, G., Wu, C., Wang, J., Li, J., Zhang, L., Han, Y., Liu, L., Cao, C., Cao, J., He, Q., and Liu, X.:  
624 Changes in concentration, composition and source contribution of atmospheric organic aerosols by shifting  
625 coal to natural gas in Urumqi, *Atmospheric Environment*, 148, 306-315, 10.1016/j.atmosenv.2016.10.053,  
626 2017.



627 Saleh, R., Hennigan, C. J., McMeeking, G. R., Chuang, W. K., Robinson, E. S., Coe, H., Donahue, N. M., and  
628 Robinson, A. L.: Absorptivity of brown carbon in fresh and photo-chemically aged biomass-burning  
629 emissions, *Atmospheric Chemistry and Physics*, 13, 7683-7693, 10.5194/acp-13-7683-2013, 2013.

630 Saleh, R., Robinson, E. S., Tkacik, D. S., Ahern, A. T., Liu, S., Aiken, A. C., Sullivan, R. C., Presto, A. A., Dubey,  
631 M. K., Yokelson, R. J., Donahue, N. M., and Robinson, A. L.: Brownness of organics in aerosols from  
632 biomass burning linked to their black carbon content, *Nature Geoscience*, 7, 647-650, 10.1038/ngeo2220,  
633 2014.

634 Satish, R. V., Shamjad, P. M., Thamban, N. M., Tripathi, S. N., and Rastogi, N.: Temporal Characteristics of  
635 Brown Carbon over the Central Indo-Gangetic Plain, *Environmental Science & Technology*, 51, 6765-6772,  
636 10.1021/acs.est.7b00734, 2017.

637 Shamjad, P. M., Satish, R. V., Thamban, N. M., Rastogi, N., and Tripathi, S. N.: Absorbing Refractive Index and  
638 Direct Radiative Forcing of Atmospheric Brown Carbon over Gangetic Plain, *ACS EARTH AND SPACE  
639 CHEMISTRY*, 2, 31-37, 10.1021/acsearthspacechem.7b00074, 2017.

640 Shen, G., Tao, S., Wei, S., Chen, Y., Zhang, Y., Shen, H., Huang, Y., Zhu, D., Yuan, C., Wang, H., Wang, Y., Pei,  
641 L., Liao, Y., Duan, Y., Wang, B., Wang, R., Lv, Y., Li, W., Wang, X., and Zheng, X.: Field measurement of  
642 emission factors of PM, EC, OC, parent, nitro-, and oxy- polycyclic aromatic hydrocarbons for residential  
643 briquette, coal cake, and wood in rural Shanxi, China, *Environ Sci Technol*, 47, 2998-3005,  
644 10.1021/es304599g, 2013.

645 Shen, Z., Zhang, Q., Cao, J., Zhang, L., Lei, Y., Huang, Y., Huang, R. J., Gao, J., Zhao, Z., Zhu, C., Yin, X.,  
646 Zheng, C., Xu, H., and Liu, S.: Optical properties and possible sources of brown carbon in PM 2.5 over  
647 Xi'an, China, *Atmospheric Environment*, 150, 322-330, 10.1016/j.atmosenv.2016.11.024, 2017.

648 Smith, J. D., Sio, V., Yu, L., Zhang, Q., and Anastasio, C.: Secondary organic aerosol production from aqueous  
649 reactions of atmospheric phenols with an organic triplet excited state, *Environmental Science & Technology*,  
650 48, 1049-1057 10.1021/es4045715, 2014.

651 Sumlin, B. J., Pandey, A., Walker, M. J., Pattison, R. S., Williams, B. J., and Chakrabarty, R. K.: Atmospheric  
652 Photooxidation Diminishes Light Absorption by Primary Brown Carbon Aerosol from Biomass Burning,  
653 *Environmental Science & Technology Letters*, 4, 540-545, 10.1021/acs.estlett.7b00393, 2017.

654 Sun, J., Zhi, G., Hitznerberger, R., Chen, Y., Tian, C., Zhang, Y., Feng, Y., Cheng, M., Zhang, Y., and Cai, J.:  
655 Emission factors and light absorption properties of brown carbon from household coal combustion in China,  
656 *Atmospheric Chemistry and Physics*, 17, 4769-4780, 10.5194/acp-17-4769-2017, 2017.

657 Teich, M., Van Pinxteren, D., Wang, M., Kecorius, S., Wang, Z., Müller, T., Močnik, G., and Herrmann, H.:  
658 Contributions of nitrated aromatic compounds to the light absorption of water-soluble and particulate brown  
659 carbon in different atmospheric environments, *Atmospheric Chemistry and Physics*, 17, 1-24,  
660 10.5194/acp-17-1653-2017, 2017.

661 Wang, D., Tian, F., Yang, M., Liu, C., and Li, Y. F.: Application of positive matrix factorization to identify  
662 potential sources of PAHs in soil of Dalian, China, *Environmental Pollution*, 157, 1559-1564,  
663 10.1016/j.envpol.2009.01.003, 2009a.

664 Wang, G., Kawamura, K., Xie, M., and Hu, S.: Size-distributions of n-hydrocarbons, PAHs and hopanes and  
665 their sources in the urban, mountain and marine atmospheres over East Asia, *Atmospheric Chemistry &  
666 Physics*, 9, 8869-8882, 10.5194/acp-9-8869-2009, 2009b.

667 Wang, G., Xie, M., Hu, S., Gao, S., Tachibana, E., and Kawamura, K.: Dicarboxylic acids, metals and isotopic  
668 compositions of C and N in atmospheric aerosols from inland China: implications for dust and coal burning  
669 emission and secondary aerosol formation, *Atmospheric Chemistry and Physics*, 10, 6087-6096,

670 10.5194/acp-10-6087-2010, 2010.

671 Wang, G., Zhang, R., Gomez, M. E., Yang, L., Zamora, M. L., Hu, M., Lin, Y., Peng, J., Guo, S., Meng, J., Li, J.,  
672 Cheng, C., Hu, T., Ren, Y., Wang, Y., Gao, J., Cao, J., An, Z., Zhou, W., Li, G., Wang, J., Tian, P.,  
673 Marrero-Ortiz, W., Secrest, J., Du, Z., Zheng, J., Shang, D., Zeng, L., Shao, M., Wang, W., Huang, Y., Wang,  
674 Y., Zhu, Y., Li, Y., Hu, J., Pan, B., Cai, L., Cheng, Y., Ji, Y., Zhang, F., Rosenfeld, D., Liss, P. S., Duce, R. A.,  
675 Kolb, C. E., and Molina, M. J.: Persistent sulfate formation from London Fog to Chinese haze, Proceedings  
676 of the National Academy of Sciences of the United States of America, 113, 13630-13635,  
677 10.1073/pnas.1616540113, 2016.

678 Wang, G. H., Zhou, B. H., Cheng, C. L., Cao, J. J., Li, J. J., Meng, J. J., Tao, J., Zhang, R. J., and Fu, P. Q.:  
679 Impact of Gobi desert dust on aerosol chemistry of Xi'an, inland China during spring 2009: differences in  
680 composition and size distribution between the urban ground surface and the mountain atmosphere,  
681 Atmospheric Chemistry and Physics, 13, 819-835, 10.5194/acp-13-819-2013, 2013.

682 Wang, J., Cao, J., Dong, Z., Guinot, B., Gao, M., Huang, R., Han, Y., Huang, Y., Ho, S., and Shen, Z.: Seasonal  
683 variation, spatial distribution and source apportionment for polycyclic aromatic hydrocarbons (PAHs) at  
684 nineteen communities in Xi'an, China: The effects of suburban scattered emissions in winter, Environmental  
685 Pollution, 1330-1343, 10.1016/j.envpol.2017.08.106, 2017.

686 Wang, X., Heald, C. L., Ridley, D. A., Schwarz, J. P., Spackman, J. R., Perring, A. E., Coe, H., Liu, D., and  
687 Clarke, A. D.: Exploiting simultaneous observational constraints on mass and absorption to estimate the  
688 global direct radiative forcing of black carbon and brown carbon, Atmospheric Chemistry and Physics, 14,  
689 17527-17583, 10.5194/acp-14-10989-2014, 2014.

690 Wu, C., Wang, G., Wang, J., Li, J., Ren, Y., Zhang, L., Cao, C., Li, J., Ge, S., and Xie, Y.: Chemical  
691 characteristics of haze particles in Xi'an during Chinese Spring Festival: Impact of fireworks burning,  
692 Journal of Environmental Sciences, 179-187, 10.1016/j.jes.2018.04.008, 2018.

693 Wu, C., Wang, G., Cao, C., Li, J., Li, J., Wu, F., Huang, R., Cao, J., Han, Y., Ge, S., Xie, Y., Xue, G., and Wang,  
694 X.: Chemical characteristics of airborne particles in Xi'an, inland China during dust storm episodes:  
695 Implications for heterogeneous formation of ammonium nitrate and enhancement of N-deposition,  
696 Environmental Pollution, 244, 877-884, 10.1016/j.envpol.2018.10.019, 2019.

697 Xie, M., Chen, X., Hays, M. D., Lewandowski, M., Offenberg, J., Kleindienst, T. E., and Holder, A. L.: Light  
698 Absorption of Secondary Organic Aerosol: Composition and Contribution of Nitroaromatic Compounds,  
699 Environmental Science & Technology, 51, 11607-11616, 10.1021/acs.est.7b03263, 2017.

700 Xie, M., Shen, G., Holder, A. L., Hays, M. D., and Jetter, J. J.: Light absorption of organic carbon emitted from  
701 burning wood, charcoal, and kerosene in household cookstoves, Environmental Pollution, 240, 60-67,  
702 10.1016/j.envpol.2018.04.085, 2018.

703 Yan, C., Zheng, M., Sullivan, A. P., Bosch, C., Desyaterik, Y., Andersson, A., Li, X., Guo, X., Zhou, T., and  
704 Örjan, G.: Chemical characteristics and light-absorbing property of water-soluble organic carbon in Beijing:  
705 Biomass burning contributions, Atmospheric Environment, 121, 4-12, 10.1016/j.atmosenv.2015.05.005,  
706 2015.

707 Yan, C., Zheng, M., Bosch, C., Andersson, A., Desyaterik, Y., Sullivan, A. P., Collett, J. L., Zhao, B., Wang, S.,  
708 He, K., and Gustafsson, O.: Important fossil source contribution to brown carbon in Beijing during winter,  
709 Scientific Reports, 7, 43182, 10.1038/srep43182, 2017.

710 Yan, J., Wang, X., Gong, P., Wang, C., and Cong, Z.: Review of brown carbon aerosols: Recent progress and  
711 perspectives, Science of The Total Environment, 634, 1475-1485, 10.1016/j.scitotenv.2018.04.083, 2018.

712 Yang, H., Xu, J., Wu, W. S., Wan, C. H., and Yu, J. Z.: Chemical Characterization of Water-Soluble Organic

713 Aerosols at Jeju Island Collected During ACE-Asia, *Environmental Chemistry*, 1, 13-17, 10.1071/EN04006,  
714 2004.

715 Yuan, B., Liggió, J., Wentzell, J., Li, S.-M., Stark, H., Roberts, J. M., Gilman, J., Lerner, B., Warneke, C., Li, R.,  
716 Leithead, A., Osthoff, H. D., Wild, R., Brown, S. S., and de Gouw, J. A.: Secondary formation of nitrated  
717 phenols: insights from observations during the Uintah Basin Winter Ozone Study (UBWOS) 2014,  
718 *Atmospheric Chemistry and Physics*, 16, 2139-2153, 10.5194/acp-16-2139-2016, 2016.

719 Zhai, J., Lu, X., Li, L., Zhang, Q., Zhang, C., Chen, H., Yang, X., and Chen, J.: Size-resolved chemical  
720 composition, effective density, and optical properties of biomass burning particles, *Atmospheric Chemistry  
721 and Physics*, 17, 1-25, 10.5194/acp-17-7481-2017, 2017.

722 Zhang, X., Hecobian, A., Zheng, M., Frank, N. H., and Weber, R. J.: Biomass burning impact on PM<sub>2.5</sub> over the  
723 southeastern US during 2007: integrating chemically speciated FRM filter measurements, MODIS fire  
724 counts and PMF analysis, *Atmospheric Chemistry and Physics*, 10, 6839-6853, 10.5194/acp-10-6839-2010,  
725 2010.

726 Zhang, X., Lin, Y. H., Surratt, J. D., Zotter, P., Prévôt, A. S. H., and Weber, R. J.: Light-absorbing soluble organic  
727 aerosol in Los Angeles and Atlanta: A contrast in secondary organic aerosol, *Geophysical Research Letters*,  
728 38, 759-775, 10.1029/2011GL049385, 2011.

729 Zhang, Y., and Tao, S.: Global atmospheric emission inventory of polycyclic aromatic hydrocarbons (PAHs) for  
730 2004, *Atmospheric Environment*, 43, 812-819, 10.1016/j.atmosenv.2008.10.050, 2009.

731 Zhang, Z., Gao, J., Engling, G., Tao, J., Chai, F., Zhang, L., Zhang, R., Sang, X., Chan, C. Y., and Lin, Z.:  
732 Characteristics and applications of size-segregated biomass burning tracers in China's Pearl River Delta  
733 region, *Atmospheric Environment*, 102, 290-301, 10.1016/j.atmosenv.2014.12.009, 2015.

734 Zhao, M., Huang, Z., Qiao, T., Zhang, Y., Xiu, G., and Yu, J.: Chemical characterization, the transport pathways  
735 and potential sources of PM<sub>2.5</sub> in Shanghai: Seasonal variations, *Atmospheric Research*, 158-159, 66-78,  
736 10.1016/j.atmosres.2015.02.003, 2015a.

737 Zhao, R., Lee, A. K. Y., Huang, L., Li, X., Yang, F., and Abbatt, J. P. D.: Photochemical processing of aqueous  
738 atmospheric brown carbon, *Atmospheric Chemistry and Physics*, 15, 6087-6100,  
739 10.5194/acp-15-6087-2015, 2015b.

740 Zong, Z., Wang, X., Tian, C., Chen, Y., Qu, L., Ji, L., Zhi, G., Li, J., and Zhang, G.: Source apportionment of  
741 PM<sub>2.5</sub> at a regional background site in North China using PMF linked with radiocarbon analysis: insight  
742 into the contribution of biomass burning, *Atmospheric Chemistry and Physics*, 16, 11249-11265,  
743 10.5194/acp-16-11249-2016, 2016.

744

745

746

747

748

749

750

751

## 752 **Table List**

753 Table 1. Concentrations of organic carbon in PM<sub>2.5</sub> and meteorological conditions during  
754 winter and summer of 2017 in Xi'an, inland China.

755  
756 Table 2. Comparison on light absorption ( $\text{abs}_{\lambda=365\text{nm}}$ ), MAC, and AAE values of water-extracts of  
757 PM<sub>2.5</sub> in Xi'an, China with those in other cities.

758  
759 Table 3. Complex refractive index ( $k$ ) of brown carbon from samples extracted by water in  
760 two seasons.

761  
762

## 763 **Figure caption**

764 Fig. 1 Temporal variations of WSOC, OC, PM<sub>2.5</sub>, and  $\text{abs}_{\lambda=365\text{nm}}$  of PM<sub>2.5</sub> samples extracted by  
765 water (H<sub>2</sub>O extraction) and methanol (MeOH extraction) during winter (**a** and **c**) and summer  
766 (**b** and **d**).

767  
768 Fig. 2 Seasonal average values of  $\text{abs}_{\lambda=365\text{nm}}$ , AAE, and MAC extracted by MeOH and H<sub>2</sub>O.  
769 AAE is calculated by linear regression fit  $\log(\text{abs}_{\lambda=365\text{nm}})$  versus  $\log(\lambda)$  in the wavelength  
770 range of 300–450 nm. (The shadows indicating the standard deviations)

771  
772 Fig. 3 Size distributions of  $\text{abs}_{\lambda=365\text{nm}}$  and MAC of PM<sub>2.5</sub> samples extracted by water during  
773 the winter and summer of 2017 in Xi'an.

774  
775 Fig. 4 An orthogonal regression analysis for  $\text{abs}_{\lambda=365\text{nm}}$  of samples between predicted by Mie  
776 theory and extracted by water for different particle size ( $D_p < 2.1\mu\text{m}$ ).

777  
778 Fig. 5 Temporal variations of PM<sub>2.5</sub>, meteorological parameters,  $\text{abs}_{\lambda=365\text{nm}}$  of W(M)SOC and  
779 organic compounds in the period of January 10<sup>th</sup>–20<sup>th</sup> (The cyan shadow indicates a haze  
780 period from January 12<sup>th</sup> to 19<sup>th</sup> with a daily PM<sub>2.5</sub> > 75  $\mu\text{g}/\text{m}^3$ ).

781 .  
782  
783 Fig.6 Linear fit regressions for the ratio of light absorption of methnoal-extracts to light  
784 absorption of EC ( $\text{abs}_{\lambda=365\text{nm}}\text{-MeOH}/\text{abs}_{\lambda=550\text{nm}}\text{-EC}$ ) with (**a** and **b**)  $\delta^{13}\text{C}$  and (**c** and **d**) relative  
785 abundance of nitrophenol to EC(Nitrophenol/EC) in the day- and night-PM<sub>2.5</sub> samples  
786 collected during the haze period of January 12<sup>th</sup> to19<sup>th</sup> (corresponding to the cyan shadow in  
787 Figure 5) in Xi'an.

788  
789 Fig. 7 Factor profiles resolved by PMF mode during the winter and summer sampling period.  
790 The bars represent the concentrations of species and the dots represent the contributions of  
791 species appointed to the factors (the summer and winter samples were merged together for the

792 PMF analysis due to the limited number of samples).

793

794 Fig. 8 Source apportionment for airborne fine particulate BrC in Xi'an during the campaign.

795

796

797

798

799

800 Table 1. Concentrations of organic carbon in PM<sub>2.5</sub> and meteorological conditions during  
801 winter and summer of 2017 in Xi'an, inland China.

	Winter	Summer
I. Mass concentrations of organic matter in PM <sub>2.5</sub>		
WSOC ( $\mu\text{gC}/\text{m}^3$ )	$23 \pm 13$	$5.8 \pm 1.4$
OC ( $\mu\text{gC}/\text{m}^3$ )	$41 \pm 25$	$8.4 \pm 2.4$
PAHs ( $\text{ng}/\text{m}^3$ )	$149 \pm 89$	$8.1 \pm 6.5$
OPAHs ( $\text{ng}/\text{m}^3$ )	$174 \pm 98$	$17 \pm 8.7$
Nitrophenols ( $\text{ng}/\text{m}^3$ )	$17 \pm 12$	$0.40 \pm 0.27$
Levoglucosan ( $\text{ng}/\text{m}^3$ )	$739 \pm 432$	$29 \pm 22$
II. PM <sub>2.5</sub> and meteorological parameters		
PM <sub>2.5</sub> ( $\mu\text{g}/\text{m}^3$ )	$194 \pm 141$	$37 \pm 16$
T ( $^{\circ}\text{C}$ )	$2.6 \pm 2.9$	$31 \pm 5.4$
RH (%)	$60 \pm 20$	$58 \pm 19$
Visibility (km)	$7.0 \pm 7.0$	$21 \pm 11$

802

803

804

805

806

807

808

809

810

811

812

813

814

815

816

817

818

819

820

821

822 Table 2. Comparison on light absorption ( $abs_{\lambda=365nm}$ ), MAC, and AAE values of water-extracts of  
 823  $PM_{2.5}$  in Xi'an, China with those in other cities.

Location	Time	$abs_{\lambda=365nm}$ (M/m)		MAC ( $m^2/g$ )		AAE		References
		Winter	Summer	Winter	Summer	Winter	Summer	
Xi'an, China	2016-2017	49±32 <sup>a</sup>	5.2±2.1 <sup>a</sup>	1.3±0.03 <sup>a</sup>	0.8 <sup>a</sup> ±0.1 <sup>a</sup>	6.1±9.7 <sup>a</sup>	5.5±8.8 <sup>a</sup>	This study
		28±16	3.5±1.7	1.2±0.06	1.1±0.2	5.3±8.5	4.8±7.7	
	2008-2009	46±20 <sup>a</sup>	8.3±2.3 <sup>a</sup>	1.3 <sup>a</sup>	0.7 <sup>a</sup>	6.0 <sup>a</sup>	6.0 <sup>a</sup>	Huang et al. (2018)
		25±12	5.0±1.3	1.7	1.0	5.7	5.7	
Beijing, China	2010-2011	10±8.6	3.7±3.8	1.3	0.5			Du et al. (2014)
	2011	10±6.9		1.2		7.3		Cheng et al. (2016)
	2013	14±5.2	4.6±2.2	1.5	0.7	5.3	5.8	Yan et al. (2015)
Nanjing, China	2015-2016	9.4 ± 4.7	3.3±2.4	1.0	0.5	6.7	7.3	Chen et al. (2018)
Guangzhou, China	2012	3.6±1.3		0.8		5.3		Liu et al. (2018)
Delhi, India	2010-2011			1.6		5.1		Kirillova et al. (2014)
	2015-2016	24±19		1.2				Satish et al. (2017)
Indo- Gangetic Plain India	2011	40 ± 18 <sup>b</sup>		1.3 <sup>b</sup>		5.1 <sup>b</sup>		Bachi et al. (2016)
		52 ± 27 <sup>c</sup>		1.3 <sup>c</sup>		5.3 <sup>c</sup>		
Seoul, Korea	2013-2013	11 <sup>a</sup>	5.8 <sup>a</sup>	0.9 <sup>a</sup>	1.5 <sup>a</sup>	5.5 <sup>a</sup>	4.1 <sup>a</sup>	Kim et al.(2016)
		7.3	0.9	1.0	0.3	5.8	8.7	
Atlanta, US	2010		0.6±0.4		1.2-0.2		3.4	Zhang et al. (2011)
Los Angeles Basin, US	2010		0.4-1.6		0.7		7.6	Zhang et al. (2013)

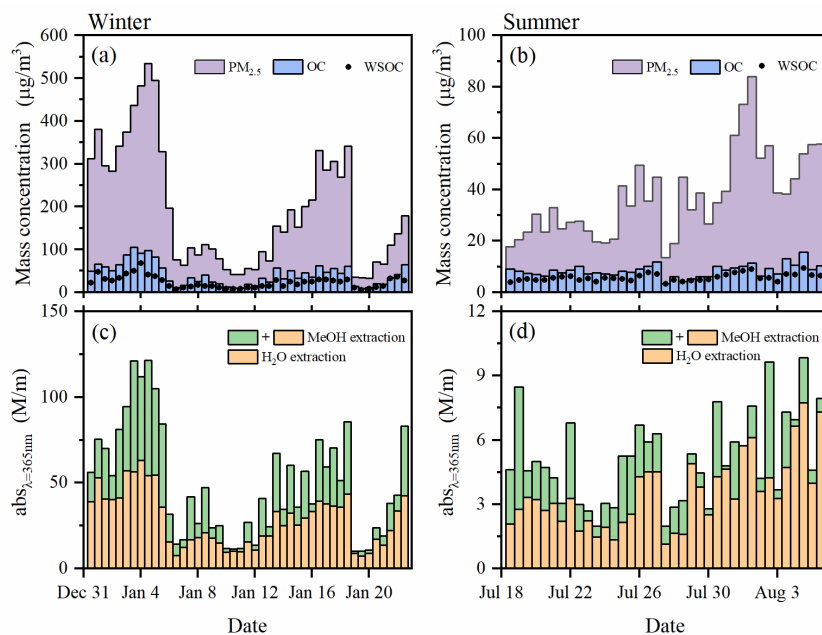
824 Notes: <sup>a</sup> solution extracted by MeOH; <sup>b</sup> samples collected at day time; <sup>c</sup> samples collected in the night

825  
826  
827  
828  
829  
830

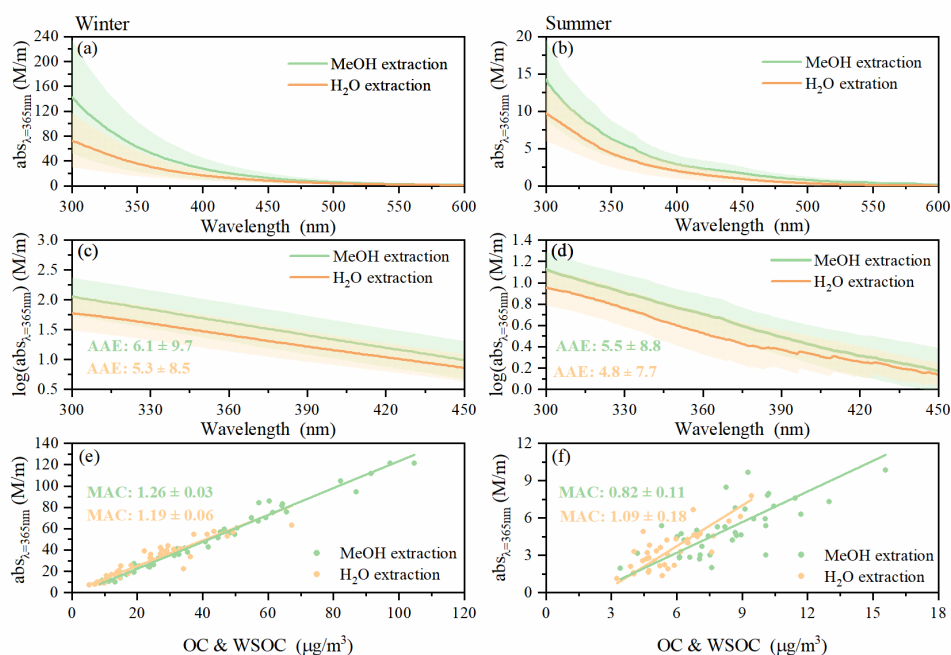
831 Table 3. Complex refractive index (k) of brown carbon from samples extracted by water in  
 832 two seasons.

Particle size ( $\mu m$ )	Winter	Summer
1.31	0.047 ± 0.005	0.021 ± 0.010
0.73	0.048 ± 0.008	0.033 ± 0.010
0.45	0.048 ± 0.013	0.031 ± 0.009
0.18	0.038 ± 0.016	0.026 ± 0.008

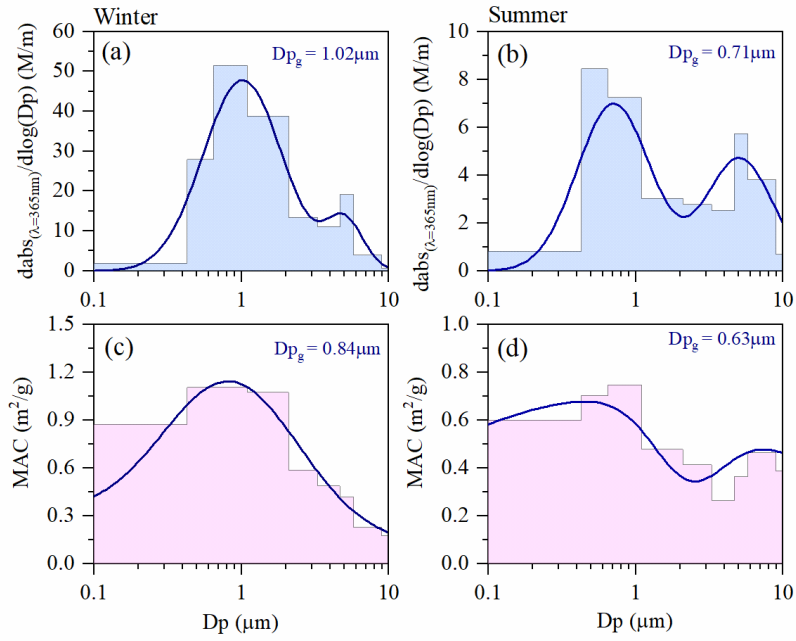
833  
834  
835



836  
 837 Fig. 1 Temporal variations of WSOC, OC, PM<sub>2.5</sub>, and  $abs_{\lambda=365nm}$  of PM<sub>2.5</sub> samples extracted by  
 838 water (H<sub>2</sub>O-extraction) and methanol (MeOH-extraction) during winter (a and c) and summer  
 839 (b and d).  
 840  
 841

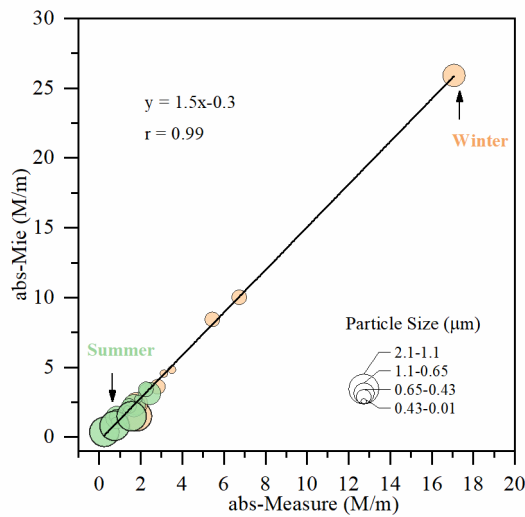


842  
 843  
 844 Fig. 2 Seasonal average values of  $abs_{\lambda=365nm}$ , AAE, and MAC extracted by MeOH and H<sub>2</sub>O.  
 845 AAE is calculated by linear regression fit  $\log(abs_{\lambda=365nm})$  versus  $\log(\lambda)$  in the wavelength  
 846 range of 300–450 nm. (The shadows indicating the standard deviations)  
 847



848  
849  
850  
851  
852  
853  
854

Fig. 3 Size distributions of  $abs_{\lambda=365nm}$  and MAC of  $PM_{2.5}$  samples extracted by water during the winter and summer of 2017 in Xi'an.

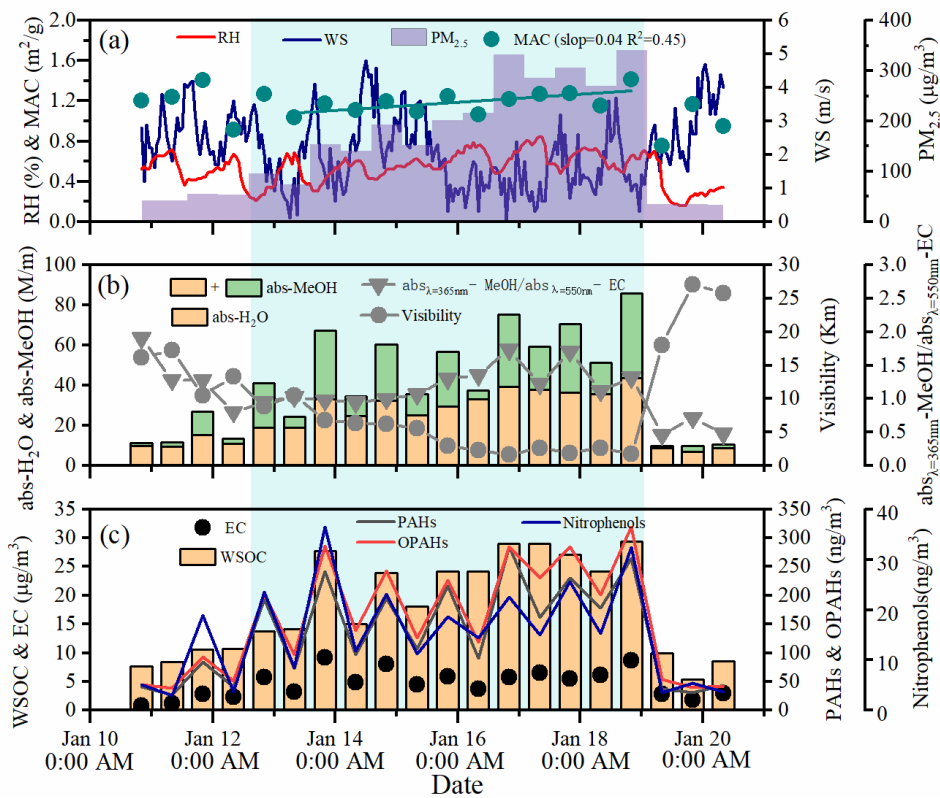


855  
856  
857  
858  
859  
860  
861  
862

Fig. 4 An orthogonal regression analysis for  $abs_{\lambda=365nm}$  of samples between predicted by Mie theory and extracted by water for different particle size ( $D_p < 2.1 \mu m$ ).

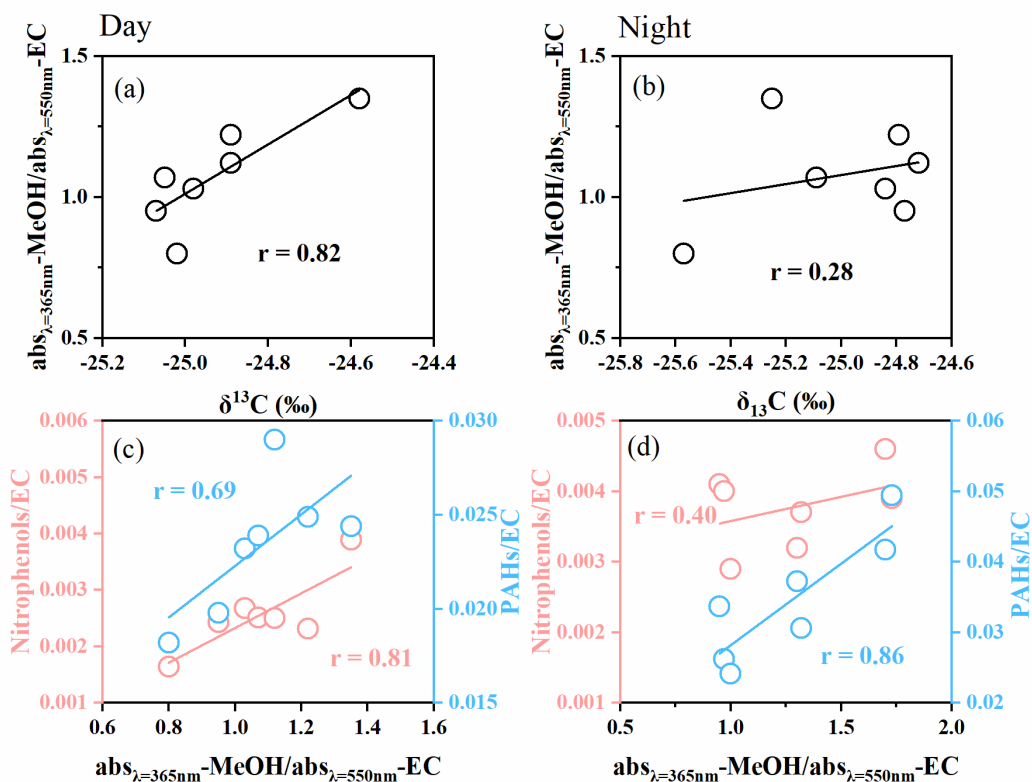


863  
 864  
 865  
 866  
 867  
 868  
 869  
 870  
 871



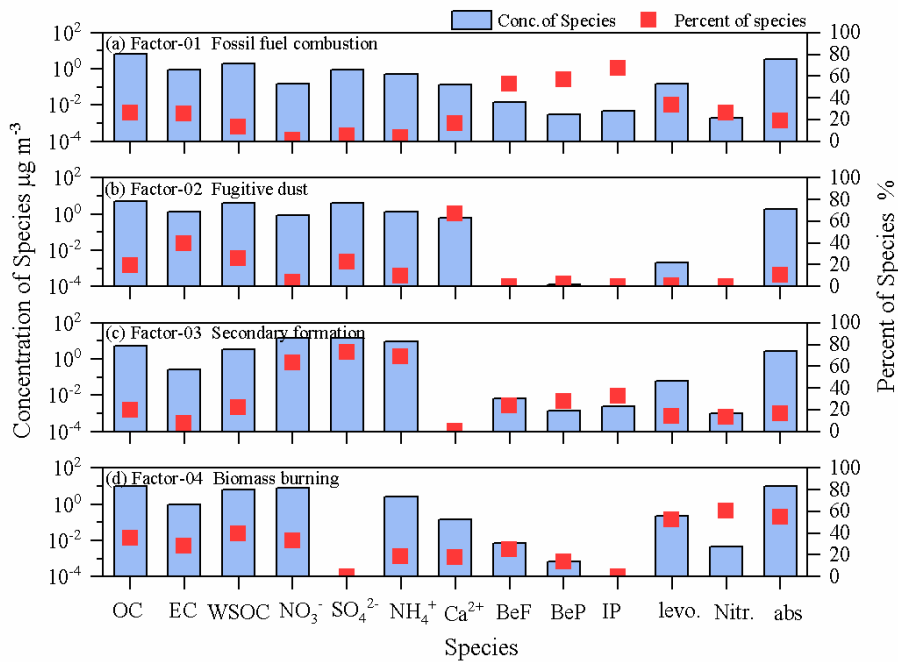
872  
 873 Fig. 5 Temporal variations of PM<sub>2.5</sub>, meteorological parameters,  $\text{abs}_{\lambda=365\text{nm}}$  of W(M)SOC and  
 874 organic compounds in the period of January 10<sup>th</sup> -20<sup>th</sup> (The cyan shadow indicates a haze  
 875 period from January 12<sup>th</sup> to 19<sup>th</sup> with a daily PM<sub>2.5</sub> > 75 μg/m<sup>3</sup>).  
 876  
 877  
 878  
 879  
 880  
 881  
 882  
 883  
 884  
 885

886  
887  
888  
889  
890  
891  
892  
893  
894  
895



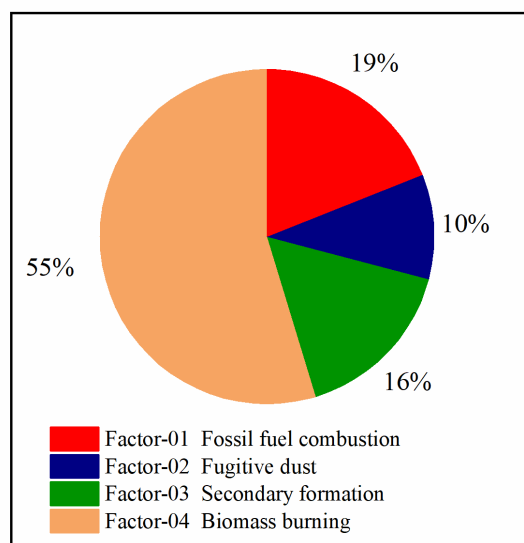
896  
897  
898  
899  
900  
901  
902  
903  
904  
905  
906  
907  
908  
909

Fig.6 Linear fit regressions for the ratio of light absorption of methanol-extracts to light absorption of EC ( $\text{abs}_{\lambda=365\text{nm}}\text{-MeOH}/\text{abs}_{\lambda=550\text{nm}}\text{-EC}$ ) with (a and b)  $\delta^{13}\text{C}$  and (c and d) relative abundance of nitrophenol to EC (Nitrophenol/EC) in the day- and night-PM<sub>2.5</sub> samples collected during the haze period of January 12<sup>th</sup> to 19<sup>th</sup> (corresponding to the cyan shadow in Figure 5) in Xi'an.



911  
 912  
 913  
 914  
 915  
 916  
 917  
 918  
 919  
 920

Fig. 7 Factor profiles resolved by PMF mode during the winter and summer sampling period. The bars represent the concentrations of species and the dots represent the contributions of species appointed to the factors (the summer and winter samples were merged together for the PMF analysis due to the limited number of samples).



921  
 922

Fig. 8 Source apportionment for airborne fine particulate BrC in Xi'an during the campaign.